ELSEVIER

Surface Science 381 (1997) 18–32

surface science

ToF-SIMS analyses of polystyrene and dibenzanthracene: evidence for fragmentation and metastable decay processes in molecular secondary ion emission

A. Delcorte *, B.G. Segda [1], P. Bertrand

Université Catholique de Louvain, PCPM, 1 Place Croix du Sud, B-1348 Louvain-la-Neuve, Belgium

Received 29 November 1996; accepted for publication 20 January 1997

Abstract

To understand the sputtering processes in unsaturated polymers, dibenzanthracene and polystyrene samples were bombarded by 15 keV, Ga^+ ions and the secondary ions were mass- and energy-analyzed by means of a time-of-flight spectrometer. The influence of various phenomena, which may play an important role in the secondary ion emission from polystyrene surfaces, is investigated: (1) emission of "original" fragments, reflecting the polymer structure; (2) emission with fragmentation, rearrangements or hydrogen losses; (3) formation of molecular ions by hydrogen or proton capture; and (4) unimolecular dissociation of the secondary ions. The dibenzanthracene molecule ($C_{22}H_{14}$) was chosen as a model compound for the study of the emission and metastable decay of polyaromatic hydrocarbon (PAH) ions under static SIMS analysis conditions. The kinetic energy distribution (KED) of most of the secondary ions sputtered from dibenzanthracene exhibits up to three peaks. The peaks corresponding to a negative apparent energy are due to the metastable decomposition of larger ions in the acceleration section of the spectrometer. Their origin, i.e. delayed H and H_2 loss reactions, is discussed in detail. The kinetic energy distributions of the dibenzanthracene secondary ions are compared with those of the PAH ions emitted from polystyrene, especially in the region $m/z = 100$–200 of the PS mass spectrum. It turns out that similar interpretations can be proposed for polystyrene. To confirm the hydrogen loss reaction in the case of polystyrene, the comparison is also made with the KED of similar but deuterated PAH ions sputtered from deuterated PS. On the basis of these hydrogen loss reactions, the formation times of the daughter ions are calculated. © 1997 Elsevier Science B.V.

Keywords: Ion emission; Metastable decay; Polystyrene; Secondary ion mass spectroscopy; Silicon; Silver; Sputtering

1. Introduction

The mechanisms of secondary ion emission from organic materials bombarded by keV ions are not yet very well known. In particular, the emission of large molecular ions from polymer surfaces is difficult to understand on the basis of simple mechanistic arguments involving atom–atom collisions [1,2]. Several theoretical and experimental methods have been proposed in order to elucidate these emission processes, e.g. collision-activated dissociation [3,4], ion beam degradation mechanisms [2,5,6], and molecular dynamics simulations [7,8]. These works have brought substantial information concerning the possible fragmentation pathways of organic (macro)molecules, but due to the indirect nature of these investigations, a ques-

* Corresponding author. Fax: (+32) 10 473452; e-mail: delcorte@pcpm.ucl.ac.be

[1] Permanent address: Département de Physique, Faculté des Sciences et Techniques (FAST), Université de Ouagadougou; P.O. Box 7021; Ouagadougou, Burkina Faso.

PII S0039-6028(97)00070-8

tion remains about their ability to model the processes correctly.

To obtain a direct insight into the physical processes leading to the secondary ion emission, the analysis of the kinetic energy distribution of the ions sputtered from various organic samples has been developed recently in our laboratory (organics [9,10] and polymers [11]). The success of this approach has been proved for a long time in the case of elemental and inorganic targets [12]. Its application to the study of organic targets has allowed us to distinguish characteristic ions, emitted by a soft emission process, from reorganized ions, resulting from a more energetic emission process [9–11]. Furthermore, correlations have been drawn between the kinetic and formation energy of the ions in the case of hydrocarbon C_xH_y fragments [10].

The case of polystyrene is already well documented with respect to the SIMS analyses: for instance, fingerprint spectrum [13], molecular weight distributions (oligomers) [14], hydrogen scrambling [15] and hydrogen transfer during emission [16], conformational effects [17], styrene-butadiene copolymers [18], and radiation damages under ion bombardment [5,19,20]. In a more specific way, measurements of the radial velocity of the C_xH_y secondary ions sputtered from polystyrene under MeV, heavy ion bombardment (electronic sputtering) have been done recently [21,22]. A periodic variation of the radial kinetic energy as a function of the number of hydrogen atoms y is observed. It is interpreted in relation to the track structure of the primary ion: unsaturated ions are originating from the hot region of the inner track whereas saturated ions are produced farther away from the track core. This is in qualitative agreement with the arguments developed in Ref. [10] for C_xH_y sputtered under keV bombardment, which is of great interest considering the very different interactions involved.

However, the way in which the highly reorganized PAH ions are formed from polystyrene surfaces is unclear. The unimolecular decomposition reactions affecting such ions are well established. The main channels of metastable decay are H, H_2 and C_2H_2 losses [23–27]. The interest developed in the decomposition reactions affecting these PAH ions has been renewed recently because of their abundance in the interstellar medium [28]. Following unimolecular reaction theory [29], the parameter governing the rate of dissociation (r) of excited species is the excess of internal energy (E_{int}) in the particle. Assuming this, rate versus energy curves can be drawn for the different reactions, allowing us to find out the dominant reaction at a given E_{int}. The lifetime of the metastable ion before dissociation is proportional to the inverse of the rate r.

For short lifetimes, typically in the range 10^{-9}–10^{-6} s, the ion fragments resulting from metastable decay can be observed in the energy spectrum of the secondary ion [30,31]. Within these lifetimes, the dissociation reaction occurs in the acceleration section of the ToF spectrometer. Therefore, the metastable ions decompose before being completely accelerated (3 kV), sharing their kinetic energy between the neutral and ion fragments in a proportion depending on the respective masses of these fragments. Consequently, the fragment ion originating from the dissociation process will be detected with a kinetic energy $E_{acc} - \Delta E_{neutral}$, lower than the kinetic energy of identical ions directly emitted from the surface. In principle, the simultaneous knowledge of the negative part of the KED and of the mass of the neutral fragment allows us to deduce the lifetime of such metastable ions [30]. It is shown in the following that such reactions may play an important role in SIMS of organic samples.

The kinetic energy distribution of several secondary ions sputtered from polystyrene has been presented elsewhere [32]. It has been observed that some PAH ions present a bimodal structure in these KEDs, which was explained by the metastable decay of larger parent ions in the acceleration section of the spectrometer. In this work, the polycyclic dibenzanthracene molecule was chosen as a model, in order to obtain a deeper understanding of the unimolecular decomposition reactions affecting PAH ions during the SIMS analysis. Indeed, the origin of the bimodal distribution in the KED of the aromatic ions emitted from polystyrene suggested the analysis of a PAH molecule

for which the parent ion could be clearly identified in the mass spectrum. The dibenzanthracene molecule, with its parent ion ($M\cdot^+$) peaking at $m/z=$ 278 in the positive mass spectrum, seemed the ideal candidate for this study. In Section 3.2, we will show how the interpretations developed to explain the behavior of the dibenzanthracene fragments may be generalized to the case of the PAH ions sputtered from polystyrene.

2. Experimental

2.1. Samples

The 1,2:5,6-dibenzanthracene sample ($C_{22}H_{14}$) was purchased from Aldrich Chem., Co. and the polystyrene sample was received from the University of Liège. It was chosen because its mass and homodispersity ($M_n=60\,000$; $H=1.05$) allowed us to neglect any effect of the chain end on the intensities of the fingerprint secondary ions [33]. The deuterated PS ($M_n=64\,000$) was received from Bayer AG (Dr. K. Reihs). The DBA powder was dissolved in acetone, and the PS beads in toluene (± 1 mg/ml). Both were prepared as thin films cast on silver substrates, by depositing a droplet of the solution on the silver substrate (0.25 cm^2) [16]. Prior to deposition, the silver substrates were etched in 25 vol.% nitric acid of analytical grade from UCB and rinsed in water of HPLC grade from a milli-Q system (Millipore). In addition, a PS sample was also cast on a cleaned silicon substrate to investigate the effect of the substrate on the secondary ion emission. The low concentration of the solutions allowed us to deposit very thin sample layers, ensuring a good electric contact between the top surface and the sample holder. To verify this, all the energy measurements were done with samples for which the substrate secondary ion peaks were present in the ToF-SIMS spectra.

2.2. SIMS analyses

The secondary ion mass analyses and the KED measurements were performed in a time-of-flight SIMS microprobe microscope (Charles Evans) using a (5 kHz) pulsed Ga^+ beam (15 kV, 400 pA DC) [34]. The angle between the gallium source and the spectrometer axis (perpendicular to the surface) is 35°. In order to avoid polymer degradation [6], the primary beam was rastered onto a (97×97 μm^2) area, allowing to keep the ion fluence below 5×10^{11} ions/cm^2 for one spectrum. For a KED measurement, ~20 spectra were recorded on the same sample area with different energy windows and the total ion fluence was kept below 10^{13} ions/cm^2.

During the secondary ion extraction periods, a $(3000-\Delta)$ V potential is applied to the sample where Δ is adjustable in order to acquire a selected part of the KED and this 3 kV corresponds to the nominal extraction voltage. The departing secondary ions are accelerated between the sample and the extraction plate (grounded entrance of the first Einzel lens) and focused before to enter a field free drift region. They are afterwards 270° deflected by three hemispherical electrostatic analyzers (ESA) before reaching the detector. At the crossover following the first ESA (at 90° with respect to the spectrometer axis), they are energy selected by a slit of fixed width (100 μm, corresponding to a passband of 1.5 eV). Thus, the detected part of the KED will correspond to the mean energy $(\Delta-C)$ eV, where C is a constant. The acquisition of mass spectra for different sample voltages allows the collection of a complete KED, a 1 V increase of the sample potential corresponding to a 1 eV decrease in the KED. An alternative way to measure the KED is to keep the sample voltage at the fixed nominal value (3 kV) and to shift the energy slit perpendicularly to the beam in order to accept different regions of the KED. The spatial distribution is then converted into an energy distribution owing to an empirical equation derived from the simulation of the ion trajectories [35]. The determination of the zero of the energy scale (C) is not trivial: it is estimated in the following from the intersection between the tangent to the increasing part of the KED of the atomic substrate ions (Si^+, Ag^+) and the energy axis. The corrected value of the sample voltage ($\Delta-C$), giving the initial kinetic energy of the secondary ions, will be called "apparent energy" in the following.

3. Results and discussion

3.1. Fingerprint ions

The positive mass spectrum of PS cast on silver (Fig. 1) exhibits the classical fingerprint peaks, well documented in the literature [36]. Most of these peaks correspond to (poly)cyclic, aromatic hydrocarbon ions (PAHs). Peaks related to the Ag substrate are also present in the mass spectrum, indicating the small thickness of the PS film. The comparison with the mass spectrum of PS cast on silicon, in the same conditions, shows that the effect of the nature of the substrate on the relative intensity of the fingerprint ions is weak.

In Fig. 2, the detected secondary ion yield of four fragments sputtered from PS is plotted as a function of the secondary ion yield of silver, for five different samples realized with the same polymer solution. The Ag^+ yield of the bare silver is indicated by the dashed line (5.25×10^{-3}). The increase in PS ion yield with Ag^+ yield in the considered range shows the effect of the substrate on PS ion formation. Below $Y^+(^{107}Ag)=4\times10^{-4}$, i.e. when the polymer covers the silver substrate sufficiently to reduce the Ag^+ intensity by a factor of 10, the yield of PS ions is nearly

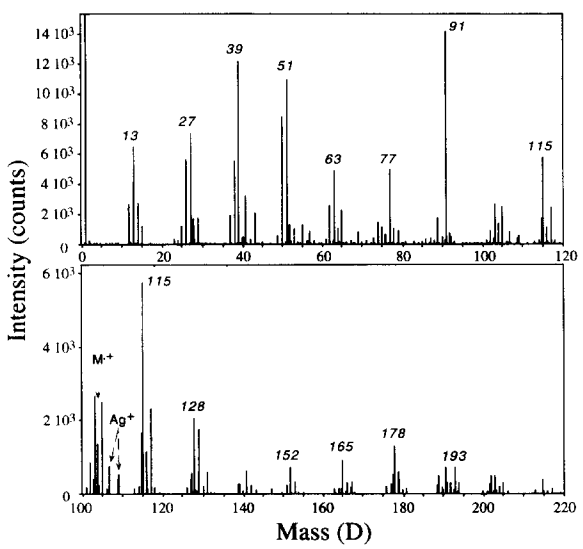

Fig. 1. Secondary ion mass spectrum of PS ($M_n=60\,000$) cast on silver.

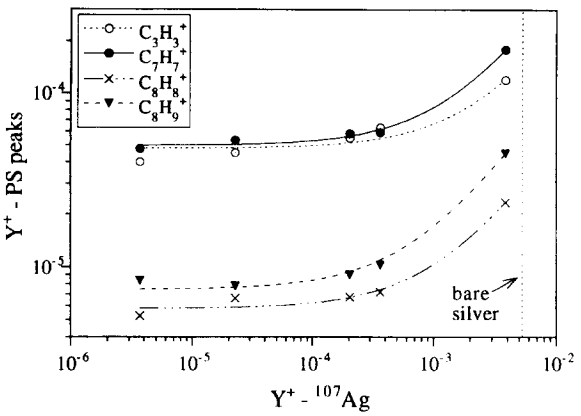

Fig. 2. Yield of the PS secondary ions as a function of the Ag secondary ion yield for five different samples cast from the same solution (1 mg ml^{-1}). The yield is calculated with the formula: Y^+ = average positive ions detected/primary particle.

constant. Thus, we can consider that the effect of the substrate is weak in this range, and that the KED measurements obtained on these samples are not drastically influenced by the underlying silver layer. In practice, all the KED measurements were realized on such samples ($Y^+(^{107}Ag)<4\times10^{-4}$). It is interesting to note that the secondary ion yield of the most intense ion in the PS spectrum, $C_7H_7^+$, ranges from 5×10^{-5} when the substrate effect is negligible, to 1.8×10^{-4} when the substrate effect is present. A detailed study of the effect of the substrate on the SI emission of organic molecules has been realized recently [37]. In this work, a positive correlation between the signal of the protonated molecule $(M+H)^+$ and the Ag substrate signal is observed with a coverage of one monolayer and more. Indeed, above one monolayer, both signals decrease drastically. Our results suggest that the same phenomenon occurs in the case of polymers. As the sputtered neutrals exhibit similar behavior [37], the explanation of this phenomenon probably lies in the sputtering process itself, and not in the ionization step of the SI emission.

For the PS sample cast on silicon, the secondary ion yields measured were: $Y^+(Si)=3.5\times10^{-4}$; $Y^+(C_3H_3)=7\times10^{-5}$; $Y^+(C_7H_7)=6\times10^{-5}$; $Y^+(C_8H_8)=8\times10^{-6}$ and $Y^+(C_8H_9)=1.2\times10^{-5}$; which are very close to the constant values measured with the silver substrate. This leads to the

conclusion that the influence of the substrate in all our KED measurements is weak, and that the features observed are intrinsically related to the ion–polymer interaction itself.

In polystyrene, the formation of several molecular ions seems rather "direct" (m/z = 39; 51; 63; 77; 103; 104; 117; 193), because it requires only bond-scissions. The KED of such ions will be presented in this section. By contrast, the emission of polycyclic ions in the range 100–200 D (m/z = 115; 128; 141; 152; 165; 178) needs an additional rearrangement, the complexity increasing with the size of the ion formed. They will be considered in Section 3.2. The case of the $C_7H_7^+$ (m/z = 91) and $C_8H_9^+$ (m/z = 105) is somewhat different: both have an excess of hydrogen in comparison with the PS molecular structure and they have to capture a hydrogen atom (or a proton) to be formed.

Fig. 3 shows the KED of two of the most characteristic ions of PS, $C_6H_5^+$ (phenyl) and $C_7H_7^+$ (tropylium), both presenting cyclic structures. The two sets of curves correspond to the two different substrates, silver and silicon. As expected, there are few differences in the shape of the KEDs when comparing the different substrates. Significant intensities are measured for negative apparent energies (before the zero of the KED). As mentioned in the introduction, this can be explained by the metastable decay of molecular ions in the acceleration section of the spectrometer (see Section 3.2). On the other hand, the slope of the high-energy tail of the KED is steeper for the tropylium ion $C_7H_7^+$. It has been shown, in the frame of the collision cascade theory, that a high translational energy corresponds also to a high internal energy of the ions, leading to a higher fragmentation probability and to a removal of the high energy tail [1,38]. Conversely, softer collisions produce slower and weakly excited ions. Following this argument, the emission of the $C_7H_7^+$ could be due to a less energetic impact than the emission of the $C_6H_5^+$. Such a narrowing of the KED could also be partially explained by the so-called "size effect", observed in the case of tricosenoic acid [9,10], i.e. the transfer of momentum to one atom of a molecule is converted both in internal and kinetic energy; the kinetic versus internal energy ratio decreases with the size of the molecule [39]. In that case, a similar initial energy transfer may lead to different widths of the KED.

To illustrate the effect of the size of the secondary ion in the case of polystyrene, Fig. 4 shows

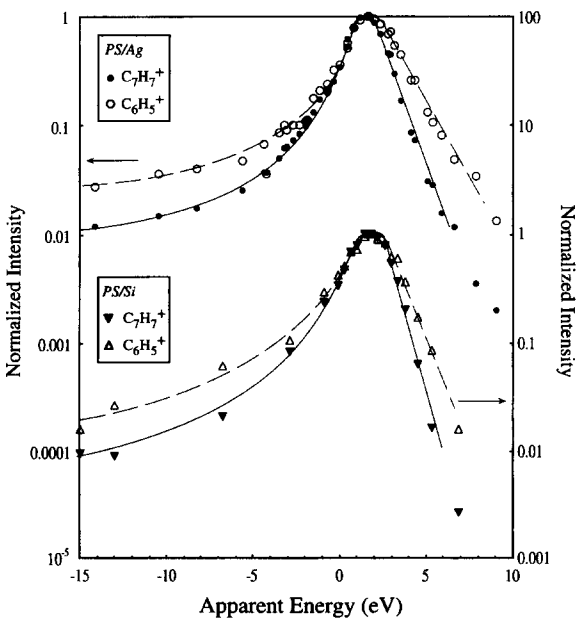

Fig. 3. Kinetic energy distribution of two "fingerprint" ions of PS, $C_6H_5^+$ (m/z = 77) and $C_7H_7^+$ (m/z = 91). Above: PS cast on silver; below: PS cast on silicon.

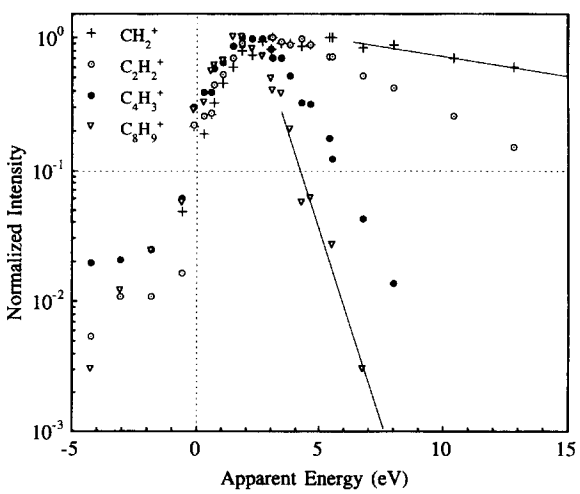

Fig. 4. Kinetic energy distribution of CH_2^+ (m/z = 14); $C_2H_2^+$ (m/z = 26); $C_4H_3^+$ (m/z = 51) and $C_8H_9^+$ (m/z = 105) sputtered from PS cast on silicon.

the KED of several molecular ions with a mass ranging from 14 to 105 D. The KED broadens when the size of the ion decreases, in a non-linear fashion. This broadening is very pronounced for low-mass ions (from CH_2^+ to $C_2H_2^+$), and tends to a lower limit when the ion mass exceeds 100 D. This behavior is qualitatively similar to the one observed with the molecular ions sputtered from tricosenoic acid [9,10].

The other important phenomenon affecting molecular ions sputtered from tricosenoic acid was the unsaturation effect. This effect can also be generalized to the case of polystyrene (Fig. 5). In each C_xH_y series, the FWHM of the distributions increases when the number of hydrogen atoms in the fragment decreases. In Ref. [10], we proposed a simple model based on the degree of similarity between the chemical and molecular structures of the secondary ions and those of the polymers. In that model, the more important is the energy transmitted to the departing ion, the higher are its internal and kinetic energies and, consequently, the deeper is its reorganization. The consequence of the reorganization is indeed to lower the excess internal energy in the ion, keeping the total kinetic energy unchanged. In this way, soft interactions produce characteristic ions with a low kinetic energy whereas violent ones give rise to reorganized ions with a higher kinetic energy. In the application of these general considerations to the case of tricosenoic acid LB films, the loss of hydrogen atoms was identified as the main fragmentation channel for the C_xH_y ions, and good correlations were found between the kinetic and formation energy of these ions [10]. It is very interesting to note that qualitatively close interpretations were developed by Papaléo et al. [21,22] to explain the periodic variation of the radial kinetic energy of the C_xH_y ions sputtered from polystyrene with very different experimental conditions (heavy MeV ion irradiation).

The FWHMs of the characteristic ions of PS confirm our interpretations (Fig. 6). In general, the ions which are close to PS structure have very narrow KEDs (($C_3H_3^+$, $C_4H_3^+$, $C_5H_5^+$, $C_6H_5^+$, $C_8H_7^+$)). The narrowest KEDs are observed for large molecular ions (size effect) or/and for secondary ions resulting most probably from hydrogen (proton) capture ($C_7H_7^+$, $C_8H_9^+$). The very narrow KEDs of this second category of ions can be explained qualitatively: indeed, the correlation in time and space which is needed for the association of the hydrogen atom (or proton) to the departing C_7H_6 and C_8H_8 ion (or neutral) fragments is consistent with a lower mean kinetic energy of this ion [40]. By contrast, very small ions or/and ions formed via hydrogen loss (unsaturation effect) exhibit broader distributions: $C_2H_2^+$, $C_3H_2^+$, $C_4H_2^+$. These observations can be interpreted in the frame of Benninghoven's model, i.e. in relation

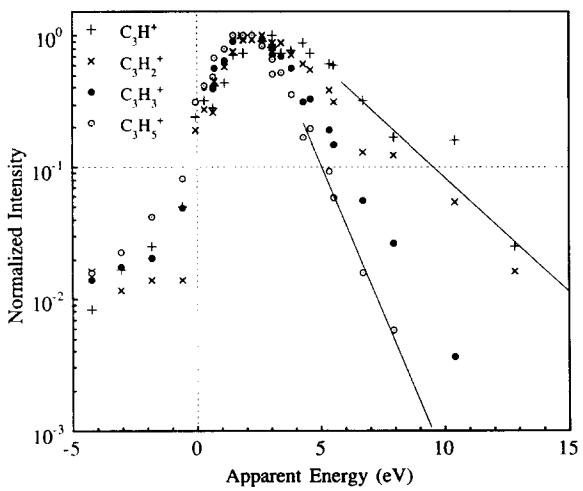

Fig. 5. Kinetic energy distribution of the $C_3H_y^+$ ions sputtered from PS cast on silicon.

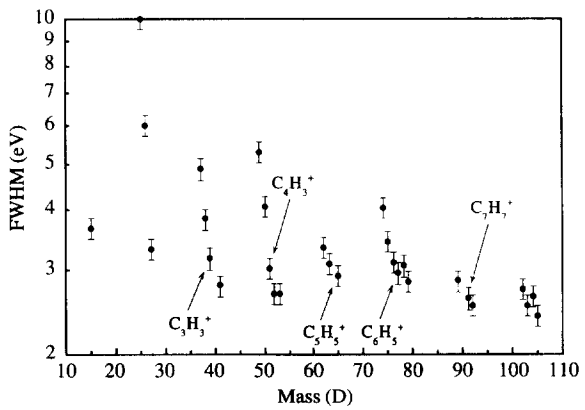

Fig. 6. FWHM of the direct emission peak of the kinetic energy distributions (C_xH_y ions sputtered from PS).

to the energy transferred to the surface species as a function of the distance r to the primary ion impact point [41]. As the energy deposited by the cascade decreases with r, our results suggest that the small and/or very unsaturated ions are produced in the high deposited energy region surrounding the impact point, whereas the larger and/or more saturated ions, reflecting the polymer structure, would be formed in a region where the deposited energy is lower and farther away from the impact point.

3.2. Metastable ions

3.2.1. Dibenzanthracene

The DBA molecule is constituted by five aromatic rings having two or four carbon atoms in common with the others (Fig. 7). This kind of PAH molecule produces rather weak fragment ion intensities under irradiation conditions [42]. The partial positive secondary ion mass spectrum of DBA is shown in Fig. 7 ($200 \leq m/z \leq 300$). The most intense peak in the mass range of the intact molecule is the parent ion $M \cdot^+$ ($C_{22}H_{14}^+$). Major peaks appear also at $m/z=276$ ($C_{22}H_{12}^+$), 277 ($C_{22}H_{13}^+$), 265 ($C_{21}H_{13}^+$) and 279 ($C_{22}H_{15}^+$), as a result of H_2, H, CH loss and H capture. The intensity of the other fragments in this region is rather weak (less than 20% of the parent ion). Above $m/z=280$, two series of peaks show significant intensities: the $C_{23}H_y^+$ series ($m/z=289$, 291) and the $C_{22}H_yO^+$ series ($m/z=293$, 294). The oxygen-containing peaks are probably due to partial oxidation of the molecule. The origin of the $C_{23}H_y^+$ series is less clear. In the interpretation of the data, it will be important to remember that the $C_{24}H_y^+$ series can not be evidenced in the mass spectrum of DBA.

Some typical KEDs of the secondary ions in the range $200 \leq m/z \leq 300$ of the DBA spectrum are shown in Figs. 8 and 9. A close look at the KED of these ions allows us to classify them into three categories: (i) distributions which do not show a well-defined peak in the "negative energy" tail (exponential tail: $m/z=280$); (ii) two peak distributions, with the second peak corresponding to a ~ 10 eV energy loss ($m/z=265$, 278, 279); (iii) three peak distributions, with the second peak

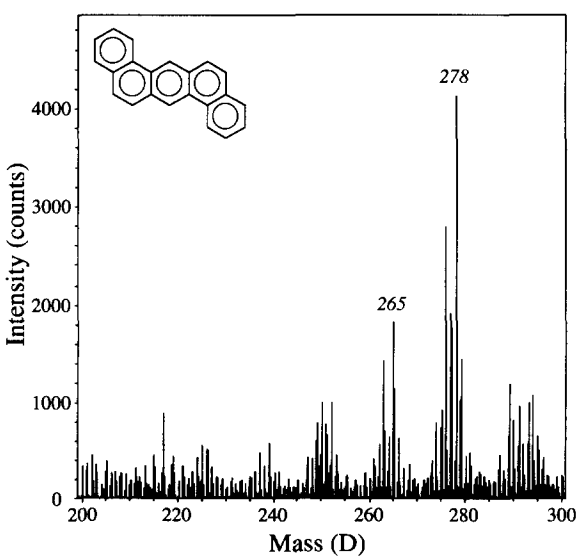

Fig. 7. Partial secondary ion mass spectrum of DBA cast on silver (200–300 D).

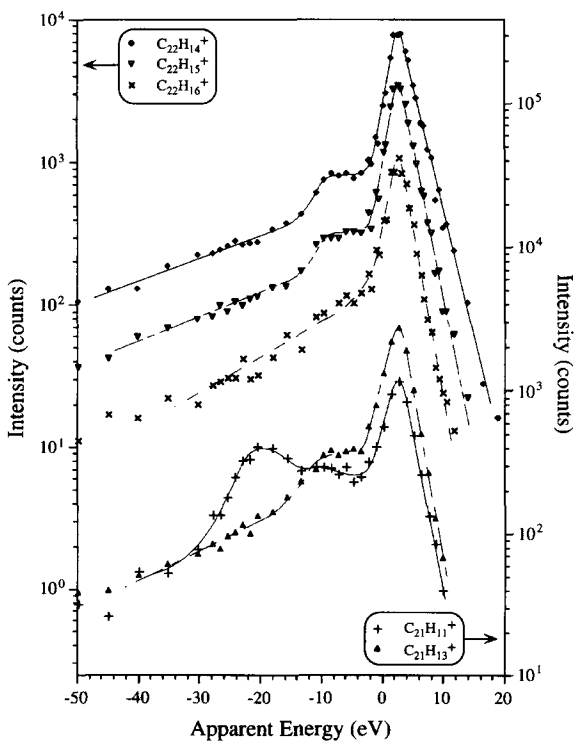

Fig. 8. Kinetic energy distribution of several secondary ions sputtered from DBA (silver substrate).

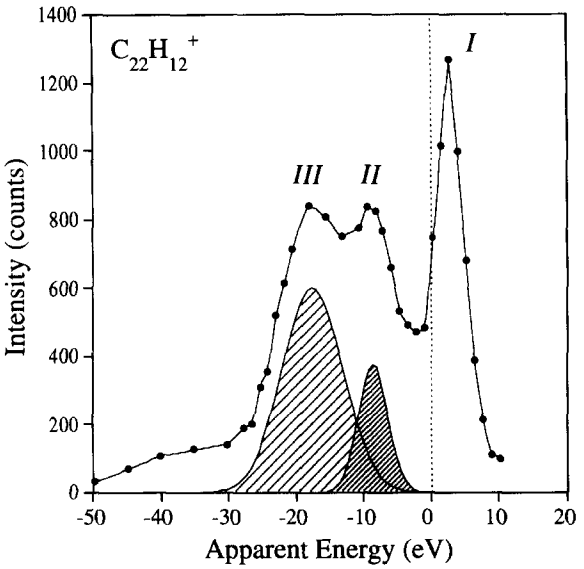

Fig. 9. Kinetic energy distribution of $C_{22}H_{12}^+$ ($m/z=276$) emitted from DBA (silver substrate). The Gaussian curves (hatched areas) indicate the calculated area of the metastable peaks.

corresponding to a 10 eV energy loss and the third peak corresponding to a ~20 eV energy loss ($m/z=263$, 276). As mentioned before, the peaks appearing in the "negative energy" tail correspond to fragments resulting from the unimolecular dissociation of their metastable parents. To explain the complex structure of the KED, two qualitatively different ion formation pathways must be considered: (a) the fast rearrangement and ionization of the molecule within the time of the collision cascade (10^{-12} s), resulting in the direct formation of the ion at the surface (direct emission peak); (b) The emission of a larger, metastable ion, followed by its decomposition far from the surface, resulting in the delayed formation of the ion (second and third peaks). The different peaks due to metastable decay would then correspond to two different reactions leading the same daughter ion.

In order to obtain a more detailed view of this phenomenon, the relative intensities of each peak of the KEDs were determined. For this purpose, an exponential baseline was subtracted in the negative part of the energy spectrum, and the two peaks corresponding to unimolecular dissociation were isolated. In first approximation, Gaussian curves were used for the peak fitting. Fig. 9 shows the result of the decomposition procedure for the peak $C_{22}H_{12}^+$ ($m/z=276$). As a result of this data treatment, the relative area of the different peaks of the energy spectra corresponding to the most intense fragments found in the mass spectrum of DBA are reported in Table 1. The intensities in Table 1 are given in percentages of the $C_{22}H_{14}^+$ ($m/z=278$) main peak intensity. For some of the ions, the metastable part of the energy spectrum is more intense than the direct emission peak. This is the case for the ions $C_{22}H_{12}^+$ ($m/z=276$) and $C_{22}H_{10}^+$ ($m/z=274$). For some other peaks, the amount of fragments resulting from metastable decay is more than 30% of the total intensity of the ion ($m/z=250$; 263; 277), which shows the importance of this process.

The relative intensities of the different metastable decay peaks may also help to explain their origin. As shown by several works using rather different techniques, the more frequent reactions for such PAH ions are hydrogen and acetylene losses [23–28,42]. In the case of DBA, it is obvious that the high intensities of the peaks due to metastable decay in the $C_{22}H_y^+$ series can not be produced by the dissociation of hypothetical $C_{24}H_{y+2}^+$ ions, which would have a much higher mass than the DBA molecule and are not present in the mass spectrum. Thus, the most probable reactions involve atomic or molecular hydrogen losses. In Fig. 10, the integrated intensity of the third peak for the ion $C_xH_{y-2}^+$ is plotted versus the direct emission peak intensity of the ion $C_xH_y^+$. The data indicate that there is a positive correlation between these two series of peaks. To understand this correlation, one must consider that the third peak of the KED of the ion $C_xH_{y-2}^+$ is the result of a H_2 loss by the metastable parent $C_xH_y^+$. Moreover, it means that the H_2 loss process contributes in a similar way for all the ions considered and constitutes a constant fraction of the parent ion intensity (~20%). Concerning the second peak, the argument related to the size of the parent ion holds too and suggests that this peak is also due to a loss of hydrogen. The fact that the less unsaturated ion of each series, $C_xH_{x-6}^+$, does not present a second peak, and that this second peak emerges for the following ion of the series, $C_xH_{x-7}^+$, is consistent with the loss of a single

Table 1
Intensity of the different components of the energy spectra (DBA on silver)

Ion Formula	Mass (m/z)	Main peak (I)	Second peak (II)	II/I (%)	Third peak (III)	III/I (%)
$C_{19}H_9^+$	237	11	1.2	*11*	1.9	*17*
$C_{19}H_{10}^+$	238	5.5	0.76	*14*	0.19	*3*
$C_{19}H_{11}^+$	239	17	0.46	*3*	0.33	*2*
$C_{19}H_{13}^+$	241	7.1	0	*0*	0	*0*
$C_{20}H_9^+$	249	7.1	1.5	*21*	1	*14*
$C_{20}H_{10}^+$	250	9.4	1.5	*16*	5	*53*
$C_{20}H_{11}^+$	251	6.1	1.3	*21*	0.9	*15*
$C_{20}H_{12}^+$	252	16	2.2	*14*	0	*0*
$C_{20}H_{13}^+$	253	8.9	0.9	*10*	0	*0*
$C_{21}H_9^+$	261	9.5	1.6	*17*	2.2	*23*
$C_{21}H_{10}^+$	262	4.7	1.9	*40*	0.3	*6*
$C_{21}H_{11}^+$	263	18	2.3	*13*	7.5	*42*
$C_{21}H_{12}^+$	264	8.4	1.4	*17*	1.4	*17*
$C_{21}H_{13}^+$	265	38	3.2	*8*	0	*0*
$C_{21}H_{14}^+$	266	14	0.7	*5*	0	*0*
$C_{22}H_{10}^+$	274	6.2	0.9	*15*	6.3	*102*
$C_{22}H_{11}^+$	275	9.8	1.3	*13*	0.5	*5*
$C_{22}H_{12}^+$	276	21	5.9	*28*	19	*90*
$C_{22}H_{13}^+$	277	13	4.1	*32*	6.9	*53*
$C_{22}H_{14}^+$	278	100	2.9	*3*	0	*0*
$C_{22}H_{15}^+$	279	45	1	*2*	0	*0*
$C_{22}H_{16}^+$	280	13	0	*0*	0	*0*
$C_{23}H_{13}^+$	289	16	1.3	*8*	3.3	*21*
$C_{23}H_{15}^+$	291	12	1.4	*12*	0	*0*
$C_{23}H_{16}^+$	292	9.9	0.8	*8*	0	*0*

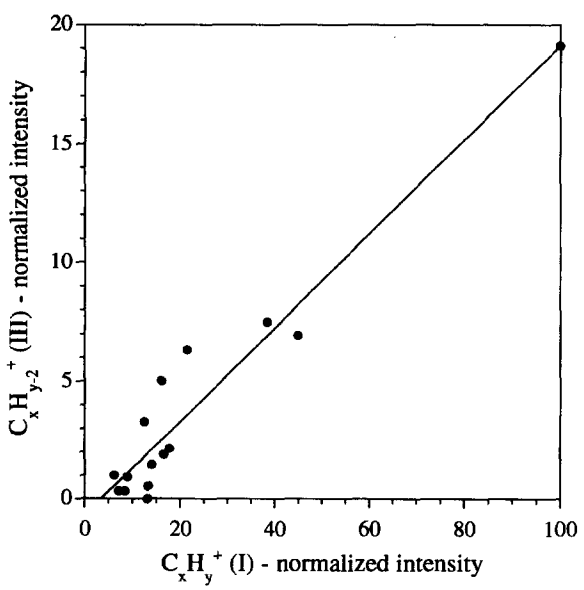

Fig. 10. Correlation between the intensity of the third peak of the ion $C_xH_{y-2}^+$ and the direct emission peak of the ion $C_xH_y^+$ ($x=19$–23), emitted from DBA.

hydrogen atom. The other ions of the series also exhibit a second peak at the same energy. However, there is no correlation between the $C_xH_{y-1}^+$ second peak intensity and the $C_xH_y^+$ first peak intensity. This lack of correlation would indicate that the fraction of metastable decay by hydrogen loss is changing with the parent ion structure.

Knowing the nature of the unimolecular reactions occurring in the acceleration section of the spectrometer, it is possible to calculate the delayed formation time of the daughter ions. In the case of the ion $C_{22}H_{12}^+$ ($m/z=276$), the considered reactions are the following:

$$C_{22}H_{13}^+(m/z=277)\rightarrow C_{22}H_{12}^+(m/z=276,\ \mathrm{II})+H, \quad (1)$$

$$C_{22}H_{14}^+(m/z=278)\rightarrow C_{22}H_{12}^+(m/z=276,\ \mathrm{III})+H_2. \quad (2)$$

As discussed before, the second peak of the KED of $C_{22}H_{12}^+$ is attributed to the first reaction,

and the third peak to the second reaction. Finally, it is assumed that, during the dissociation, the kinetic energy is shared between the two fragments in proportion of their respective masses. With these hypotheses, the average kinetic energy transferred to the H neutral (ΔK) in Eq. (1) is 8.5 eV, whereas the average kinetic energy left to the H_2 molecule in Eq. (2) is 18 eV. These correspond respectively to 2380 and 2460 eV kinetic energies for the parent ions at the dissociation point (80% of the total acceleration). Knowing the mass and the kinetic energy of the precursor at the dissociation point, the formation time of the daughter ion is determined according to the equation of the ion motion within the electric field: If the mass of the metastable ion before dissociation is m and the mass of the neutral lost is Δm, the difference of kinetic energy between an ion of mass $m-\Delta m$, formed at the surface and completely accelerated, and a similar ion resulting from metastable decay at a distance d of the surface is:

$$\Delta K = \frac{qV}{l}\frac{\Delta m}{m}d, \tag{3}$$

where q is the electron charge, V is the acceleration voltage and l is the length of the acceleration section. As ΔK is given by the experiment, it is easy to determine d by this equation. The dissociation time is then obtained from:

$$t = \sqrt{\frac{2ml}{qV}}d. \tag{4}$$

The initial kinetic energy of the ion, very small in comparison with the acceleration energy, is neglected in these equations. After this treatment, the two peaks (II and III) which were initially separated in energy, appear superimposed when plotted as a function of time (Fig. 11). The mean calculated formation time of the daughter ions for both reactions is close to 1.5×10^{-7} s. Thus, ignoring the internal energies involved in these processes, the formation times calculated with the above assumptions suggest that the two reaction channels are competitive. Similar formation times are observed for all the daughter ions resulting from the dissociation of the DBA charged fragments.

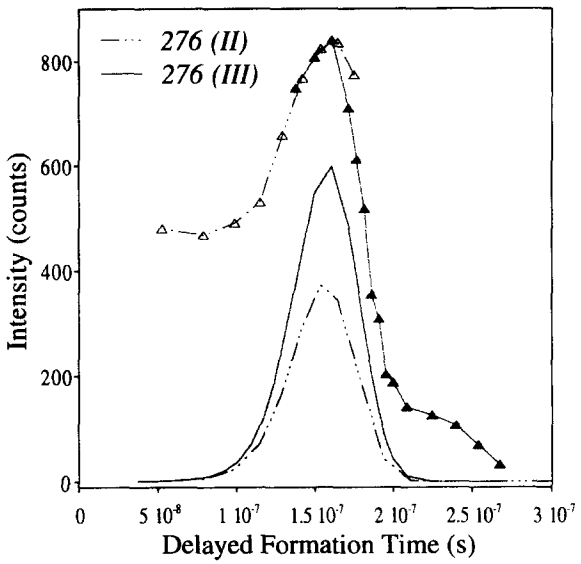

Fig. 11. Calculated formation time of the $C_{22}H_{12}^{+}$ ions resulting from unimolecular decomposition reactions.

Several of the H-loss reactions identified in Table 1 do not verify the even-electron rule [43]. According to this general rule, the reactions in which the decomposition of an even-electron ion (odd mass for the C_xH_y ions) leads to the formation of an odd-electron ion (even mass for the C_xH_y ions), are statistically unfavored. However, it has been shown by metastable decay analyses that such reactions occurred in the case of the PAH ions. In the study of the benzopyrene molecule ($C_{20}H_{12}$) [24], the reactions $m/z=251 \rightarrow m/z$ 250 and $m/z=253 \rightarrow m/z=252$ are evidenced as major reactions for these ions. On the other hand, the fact that such odd-electron hydrocarbon ions are produced by fragmentation of the DBA molecule at the surface and constitute important peaks in the mass spectrum ($m/z=252$; $m/z=276$) shows that their formation is energetically favorable. The high stability of such ions is due to the delocalization of the unpaired electron on the whole ion. Their formation enthalpy is also very low [44].

Our data do not exclude other channels of metastable decay (loss of C_2H_2, etc.), but they are not observed in the energy range analyzed. For similar lifetimes as those corresponding to the hydrogen loss reactions, a simple calculation shows that the kinetic energy left to the acetylene frag-

ment after the reaction $C_{22}H_{14}^+ \rightarrow C_{20}H_{12}^+ + C_2H_2$ would be more than 200 eV. Therefore, the centroid of the peak would be located at −200 V in the energy spectrum, and its FWHM would exceed 100 V. Due to this broadening, the peaks of this kind, even if they have a similar integrated intensity as the metastable peaks due to hydrogen loss, would be lost in the background noise and thus impossible to evidence.

3.2.2. Polystyrene

Fig. 12 shows the KED of several PAH ions sputtered from polystyrene. They all exhibit a clear, intense peak in the positive range of the spectrum, indicating that the main emission process for these ions occurs in the surface region, before any acceleration. The shape of the main peaks in Fig. 12 are not significantly different from each other, but the fast intensity decay with increasing energy is consistent with the size effect quoted in Section 3.1. A rather pronounced second peak is also present in the "negative tail" of the KED, showing a delayed formation channel for these ions (metastable decay). The KED of $C_9H_7^+$ ($m/z=115$) even shows a third peak, which will be discussed later. This delayed formation channel is consistent with a lower internal energy transfer during the emission of the parent ion. An interesting feature of these distributions is that the centroid of the second peak is shifted away from the main peak when the size of the ion decreases. This is accompanied by a simultaneous broadening of the peak. To quantify the contributions of the different formation channels for each secondary ion, the procedure developed for the DBA energy spectra was applied to the PS ions. The intensity of the different contributions (area of the peaks) for the most characteristic ions of polystyrene is indicated in Table 2. All the intensities in Table 2 are indicated in percents of the $C_7H_7^+$ main peak. The metastable contribution corresponding to the second peak exceeds 30% of the direct emission peak in two cases: $C_{12}H_8^+$ ($m/z=152$) and $C_{15}H_{11}^+$ ($m/z=191$), and it is also very important for $C_7H_5^+$ ($m/z=89$), $C_{10}H_8^+$ ($m/z=128$), $C_{11}H_9^+$ ($m/z=141$) and $C_{13}H_9^+$ ($m/z=165$).

Based on the results obtained on DBA, the second peak is attributed to a H loss. To confirm the origin of the second and third peaks in these energy spectra, a 98% deuterated polystyrene sample was prepared and analyzed in the same way. The KED of the characteristic ions of deuterated PS provides information about the nature of the reaction. Assuming that the same reactions affect hydrogenated and deuterated fragments and that they occur within similar time scales, one

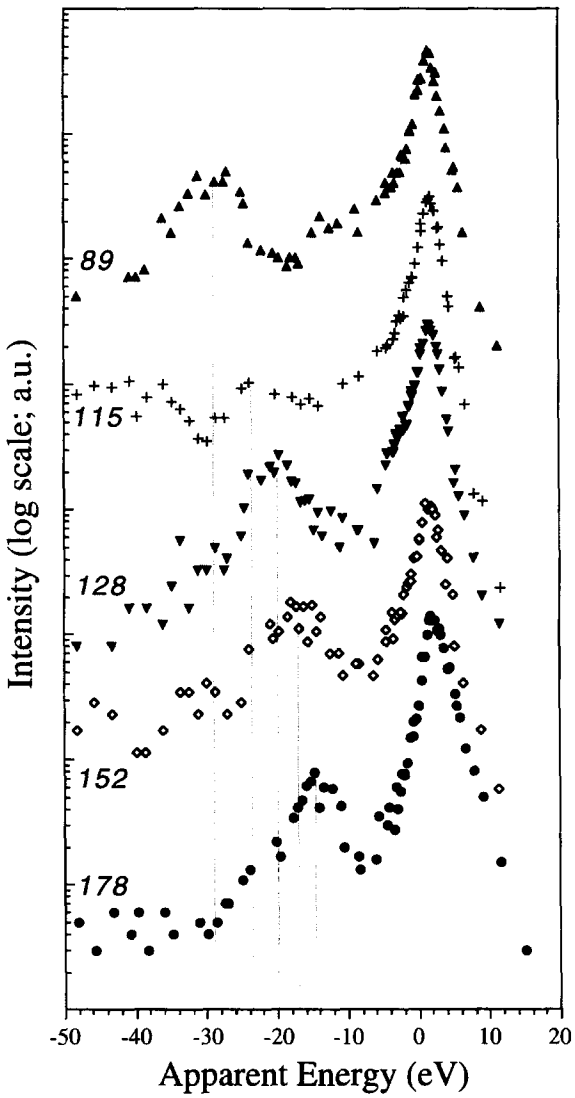

Fig. 12. Kinetic energy distribution of several polycyclic aromatic ions sputtered from PS (cast on silver). Top to bottom: $C_7H_5^+$ ($m/z=89$); $C_9H_7^+$ ($m/z=115$); $C_{10}H_8^+$ ($m/z=128$); $C_{12}H_8^+$ ($m/z=152$); $C_{14}H_{10}^+$ ($m/z=178$).

Table 2
Intensity of the different components of the energy spectra (PS on silver)

Ion Formula	Mass (m/z)	I	II	II/I (%)
$C_6H_5^+$	77	22	0.95	4
$C_7H_5^+$	89	11	2.9	26
$C_7H_7^+$	91	100	1.1	1
$C_8H_7^+$	103	17	0.49	3
$C_8H_9^+$	105	25	0	0
$C_9H_7^+$	115	30	1.3	4
$C_9H_9^+$	117	27	0	0
$C_{10}H_8^+$	128	17	2.7	16
$C_{11}H_9^+$	141	5.9	1.1	19
$C_{12}H_8^+$	152	4.2	1.5	36
$C_{13}H_9^+$	165	6.9	1.2	17
$C_{14}H_{10}^+$	178	35	2.6	7
$C_{15}H_{11}^+$	191	4.6	1.9	41
$C_{15}H_{13}^+$	193	20	0.84	4

would expect a shift of the centroid of the metastable peak in the KEDs for similar fragments. This is explained by the difference of the fragment masses, and thus by a difference in the relative fractions of the kinetic energy transferred to the daughter fragments when the metastable parent splits. Fig. 13 shows the KED of the ion $C_{14}D_{10}^+$ ($m/z=188$) sputtered from deuterated PS. The second peak is obviously shifted towards a lower energy, approximately -30 V, whereas the corresponding peak in the KED of $C_{14}H_{10}^+$ was located at -15 V. This large shift can not be explained by the small mass difference between C_xH_y and C_xD_y unsaturated ions. By contrast, the loss of D instead of H, or D_2 instead of H_2, would lead to such an important shift. This can be easily understood if one considers the following equation:

$$\frac{\Delta K}{K}\frac{m}{\Delta m}=\frac{d}{l}. \tag{5}$$

If the dissociation times are similar, the distance of dissociation d will be less than 10% smaller for $C_{14}D_{10}^+$ ($m/z=188$) than for $C_{14}H_{10}^+$ ($m/z=178$). As Δm is twice as large for D or D_2 losses as for H or H_2 losses, ΔK must be nearly twice as high for the loss of deuterium by $C_{14}D_{10}^+$ as for the loss of hydrogen by $C_{14}H_{10}^+$. Several arguments can lead us to choose between the loss of H (D) and the loss of H_2 (D_2). Once more, let us consider the case of the anthracene ion $C_{14}H_{10}^+$. Its structure is very similar to that of the dibenzanthracene parent ion (see Section 3.1), and the intensity of the peak $C_{14}H_{12}^+$ ($m/z=180$) is very weak, as was the case for the ion $C_{22}H_{16}^+$ ($m/z=280$) in the mass spectrum of DBA. Thus, the reaction $C_{14}H_{12}^+ \rightarrow C_{14}H_{10}^+ + H_2$ does not seem a good candidate to explain the second peak in the KED of $C_{14}H_{10}^+$, and this kind of reaction was not observed in the case of DBA. On the other hand, $C_9H_7^+$ ($m/z=115$) and $C_8H_7^+$ ($m/z=103$) are the only ions showing a third peak in the energy range considered in Fig. 12. Assuming that the second peak is due to a single H loss and that the third peak is due to a H_2 loss, one can calculate a mean decomposition time equal to 1.1×10^{-7} s for both reactions in the case of $C_9H_7^+$. The same observation is valid for $C_8H_7^+$. The similarity with the case of the ion $C_{22}H_{12}^+$ in DBA is clear: the same intense neighbor at mass $m/z+2$, similar reaction times for H and H_2 loss mechanisms; which is again in favor of the single H loss mechanism for the interpretation of the second peak of the KED. The fact that the series of increasing energy shift of the second peaks in Fig. 12 includes the second peak

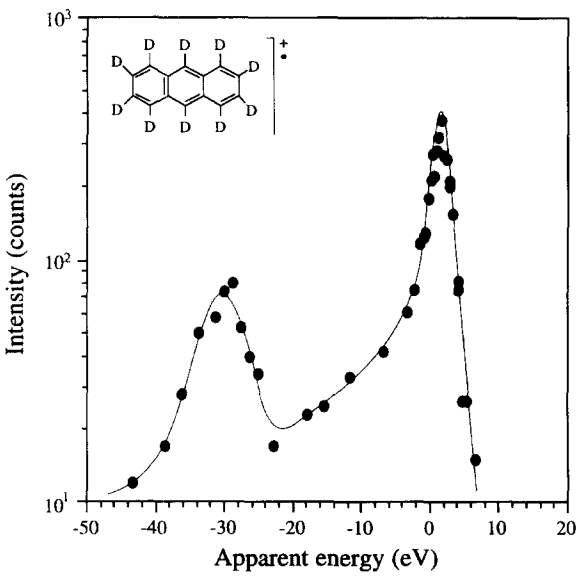

Fig. 13. Kinetic energy distribution of the polycyclic aromatic ion $C_{14}D_{10}^+$ ($m/z=188$), sputtered from deuterated PS cast on silver.

of the KED of $C_9H_7^+$ ($C_8H_7^+$), and not the third, is again in favor of a similar H loss reaction for all the ions considered. Thus, our results suggest that the predominant metastable decay channel giving rise to intense secondary peaks for the PAH ions in the case of polystyrene is the loss of one hydrogen atom. For this H loss reaction, the average formation times of the daughter ions are: 9.5×10^{-8} s for $C_7H_5^+$, 1.1×10^{-7} s for $C_9H_7^+$ and $C_{10}H_8^+$, 1.2×10^{-7} s for $C_{12}H_{10}^+$ and 1.3×10^{-7} s for $C_{14}H_{10}^+$. Calculations modeling the H loss from naphthalene ($C_{10}H_8^+$) and anthracene ($C_{14}H_{10}^+$) show that the 10^7 s^{-1} rates correspond to 10–12 eV internal energies for this reaction [27].

In parallel to the fragmentation pattern proposed by Leggett et al. for PS [4], a careful study of the C_xH_y ion energy spectra allows us to compile a table containing all the metastable decay reactions evidenced in this work. In Scheme 1, the most important reactions are indicated by full arrows, whereas the secondary reaction, corresponding to weak daughter ion intensities, are indicated by dashed arrows. The ions for which the ratio metastable peak intensity versus direct emission peak intensity is the highest are underlined. These ions exhibit a weak total intensity, and are not considered as fingerprint peaks in the PS spectrum ($m/z=164$; 190; 202). In general, the metastable decay reactions involve nearly all the C_xH_y ions in the range $m/z=100$–200 of the PS spectrum. However, the contribution of metastable H loss reactions is more pronounced for the larger ion sizes. The only H_2 loss reactions evidenced are $C_8H_9^+\rightarrow C_8H_7^+ + H_2$ and $C_9H_9^+\rightarrow C_9H_7^+ + H_2$. It is interesting to note that the main reactions occurring in the C_6, C_7, C_8, C_9 and C_{11} series verify the even-electron rule. At higher mass, the rule is no longer observed, especially when the major peak of the series corresponds to a very stable, odd-electron ion ($m/z=128$, 152, 178). The reason for this behavior has been discussed in Section 3.2.1.

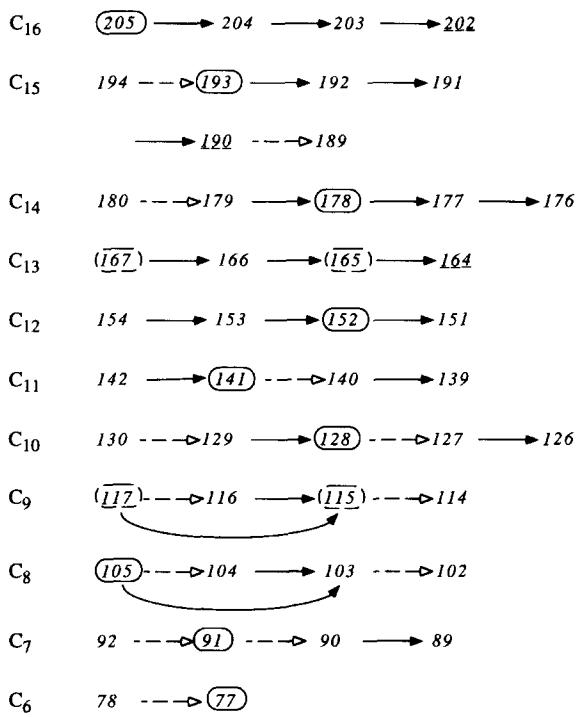

Scheme 1. Metastable decay by loss of hydrogen. Synthesis of the reactions involving the C_xH_y ions in PS. The full arrows indicate important reactions, giving rise to significant daughter-ion intensities. The dashed arrows correspond to secondary reactions, with weak (but obvious) daughter-ion intensities. The boxed numbers indicate the most intense peak in each C_xH_y series.

4. Conclusions

The energy spectra measured for molecular ions sputtered from polystyrene are interpreted on the basis of the chemical structure of the target, including the concept of internal energy-dependent fragmentation of the secondary ions. These arguments account for the direct emission peak of the KED, resulting from fast bond-scission/reorganization processes.

On the other hand, the unimolecular dissociation of metastable ions constitutes a delayed but important channel leading to the formation of fingerprint ions in the case of dibenzanthracene and polystyrene under SIMS analysis conditions. The metastable decay via atomic or molecular hydrogen loss was identified in both cases, by the comparison between the parent and daughter ion intensities (DBA), and by the comparison with the results obtained with a deuterated sample (PS). In polystyrene, the formation of fingerprint PAH ions (range 100–200 D) by metastable decay seems

mainly due to a single hydrogen atom loss. The metastable contribution can reach 25% of the total ion intensity for some secondary ions ($C_{12}H_8^+$, $C_{15}H_{11}^+$). In DBA, the metastable contribution is even more drastic for some intense secondary ions ($C_{20}H_{12}^+$, $C_{20}H_{13}^+$), reaching up to 50% of these ion intensities. The calculated formation times of the daughter ions are in the range $1–1.5\times10^{-7}$ s for both H and H_2 losses. The practical implication of these results is that the metastable ions cause artefacts in the secondary ion mass spectra (broadening and shift of the peak centroid), leading to wrong identifications.

Acknowledgements

The authors wish to thank Prof. R. Jérôme at the University of Liège for providing the PS beads, as well as Dr. K. Reihs from Bayer AG for providing the deuterated PS sample. S. Errkiba is acknowledged for her contribution to the measurements and data processing.This work and A. Delcorte are supported by the "Action de Recherche Concertée" (94/99-173) of the "Communauté Française de Belgique, Direction Générale de l'Enseignement Supérieur et de la Recherche Scientifique". The ToF-SIMS equipment was acquired with the support of the "Région Wallonne" and "FRFC- Loterie Nationale" of Belgium.

References

[1] S.J. Pachuta, R.J. Cooks, Chem. Rev. 87 (1987) 647.
[2] G.J. Leggett, J.C. Vickerman, Int. J. Mass Spectrom. Ion Proc. 122 (1992) 281.
[3] G.C. Leggett, J.C. Vickerman, in: A. Benninghoven (Ed.), Proceedings of SIMS VIII, Wiley, New York, 1991, p. 17.
[4] G.J. Leggett, J.C. Vickerman, D. Briggs, M.J. Hearn, J. Chem. Soc. Faraday. Trans. 88 (1992) 297.
[5] D. Briggs, M.J. Hearn, Vacuum 36 (1986) 1005.
[6] A. Delcorte, L.T. Weng, P. Bertrand, Nucl. Instrum. Meth. B 100 (1995) 213.
[7] R.S. Taylor, B.J. Garrison, Langmuir 11 (1995) 1220.
[8] R.S. Taylor, B.J. Garrison, Int. J. Mass Spectrom. Ion Proc. 143 (1995) 225.
[9] A. Delcorte, P. Bertrand, Nucl. Instrum. Meth. B 115 (1996) 246.
[10] A. Delcorte, P. Bertrand, Nucl. Instrum. Meth. B 117 (1996) 235.
[11] A. Delcorte, P. Bertrand, presented at SIMS X, Münster 10/95; Proc. SIMS X, Wiley, New York, p. 731.
[12] G. Betz, K. Wien, Int. J. Mass Spectrom. Ion Proc. 140 (1994) 1.
[13] D. Briggs, Surf. Interface Anal. 4 (1982) 151.
[14] I.V. Bletsos, D.M. Hercules, D. vanLeyen, B. Hagenhoff, E. Niehuis, A. Benninghoven, Anal. Chem. 63 (1991) 1953.
[15] A. Chilkoti, D.G. Castner, B.D. Ratner, Appl. Spectrosc. 45 (1991) 209.
[16] L.R. Hittle, A. Proctor, D.M. Hercules, Anal. Chem. 66 (1994) 108.
[17] X. Vanden Eynde, L.T. Weng, P. Bertrand, Surf. Interface Anal. 25 (1997) 41.
[18] L.T. Weng, P. Bertrand, W. Lauer, R. Zimmer, S. Busetti, Surf. Interface Anal. 23 (1995) 879.
[19] A. Brown, J.A. Van den Berg, J.C. Vickerman, Spectrochim. Acta B 40 (1985) 871.
[20] A. Licciardello, S. Pignataro, A. Leute, A. Benninghoven, Surf. Interface Anal. 20 (1993) 549.
[21] R.M. Papaléo, G. Brinkmalm, D. Fenyö, J. Eriksson, H.-F. Kammer, P. Demirev, P. Hakansson, B.U.R. Sundqvist, Nucl. Instrum. Meth. B 91 (1994) 667.
[22] R.M. Papaléo, P. Demirev, J. Eriksson, P. Hakansson, B.U.R. Sundqvist, Phys. Rev. B 54 (1996) 3173.
[23] L.P. Hills, J.H. Futrell, A.L. Wahrhaftig, J. Chem. Phys. 51 (1969) 5255.
[24] R.C. Lao, R.S. Thomas, J.L. Monkman, R.F. Pottie, in: A.R. West (Ed.), Advances in Mass Spectrometry, vol. 6, Applied Science, Essex, 1974, p. 129.
[25] B. Shushan, S.H. Safe, R.K. Boyd, Anal. Chem. 51 (1979) 156.
[26] H.W. Jochims, H. Rasekh, E. Rühl, H. Baumgärtel, S. Leach, Chem. Phys. 168 (1992) 159.
[27] Y. Gotkis, M. Oleinikova, M. Naor, C. Lifshitz, J. Phys. Chem. 97 (1993) 12282.
[28] T. Allain, S. Leach, E. Sedlmayr, Astron. Astrophys. 305 (1996) 602.
[29] W. Forst, Theory of Unimolecular Reactions, Academic Press, New York 1973.
[30] N.K. Dzhemilev, U.Kh. Rasulev, S.V. Verkhoturov, Nucl. Instrum. Meth. B 29 (1987) 531.
[31] N.K. Dzhemilev, A.M. Goldenberg, I.V. Veriovkin, S.V. Verkhoturov, Nucl. Instrum. Meth. B 114 (1996) 245.
[32] A. Delcorte, P. Bertrand, presented at IISC 11, Wangeroge 9/96.
[33] X. Vanden Eynde, L.T. Weng, P. Bertrand, presented at SIMS X, Münster 10/95; Proc. SIMS X, Wiley, New York, 1997, p. 727.
[34] B.W. Schueler, Microsc. Microanal. Microstruct. 3 (1992) 119.
[35] B.W.Schueler, private communication.
[36] D. Briggs, A. Brown, J.C. Vickerman, Handbook of Static Secondary Ion Mass Spectrometry (SIMS), Wiley, Chichester, 1989.
[37] R. Möllers, A. Schnieders, G. Kortenbruck, A. Benningho-

ven, presented at SIMS X, Münster 10/95; Proc. SIMS X, Wiley, New York, 1997, p. 943.
[38] A.W. Kolfschoten, R.A. Haring, A. Haring, A.E. de Vries, J. Appl. Phys. 55 (1984) 3813.
[39] H.M. Urbassek, Nucl. Instrum. Meth. B 18 (1987) 587.
[40] G.M. Lancaster, F. Honda, Y. Fukuda, J.W. Rabalais, J. Am. Chem. Soc. 101 (1979) 1951.
[41] A. Benninghoven, in: A. Benninghoven (Ed.), Ion Formation from Organic Solids, Springer, Berlin, 1982, p. 77.
[42] S.J. Pachuta, H.I. Kenttämaa, T.M. Sack, R.L. Cerny, K.B. Tomer, M.L. Gross, R.R. Pachuta, R.G. Cooks, J. Am. Chem. Soc. 110 (1988) 657.
[43] F.W. McLafferty, Interpretation of Mass Spectra, University Science Books, Mill Valley, 1980.
[44] S.G. Lias, J.E. Bartness, J.F. Liebmann, J.L. Holmes, R.D. Levin, W.G. Mallard, in: D.R. Lide Jr. (Ed.), Gas Phase Ion and Neutral Thermochemistry; ACS and AI Physics for the National Bureau of Standards, New York, 1988.